

THE SPACE DENSITY OF COMPTON THICK AGN AND THE X-RAY BACKGROUND

E. TREISTER^{1,2,3}, C. MEGAN URRY^{4,5,6} AND SHANIL VIRANI^{5,6}
ApJ in press, Feb 3, 2009

ABSTRACT

We constrain the number density and evolution of Compton-thick Active Galactic Nuclei (AGN). In the local Universe we use the wide area surveys from the Swift and INTEGRAL satellites, while for high redshifts we explore candidate selections based on a combination of X-ray and mid-IR parameters. We find a significantly lower space density of Compton-thick AGN in the local Universe than expected from published AGN population synthesis models to explain the X-ray background. This can be explained by the numerous degeneracies in the parameters of those models; we use the high-energy surveys described here to remove those degeneracies. We show that only direct observations of CT AGN can currently constrain the number of heavily-obscured supermassive black holes. At high redshift, the inclusion of IR-selected Compton-thick AGN candidates leads to a much higher space density, implying (a) a different (steeper) evolution for these sources compared to less-obscured AGN, (b) that the IR selection includes a large number of interlopers, and/or (c) that there is a large number of reflection-dominated AGN missed in the INTEGRAL and Swift observations. The contribution of CT AGN to the X-ray background is small, $\sim 9\%$, with a comparable contribution to the total cosmic accretion, unless reflection-dominated CT AGN significantly outnumber transmission-dominated CT AGN, in which case their contribution can be much higher. Using estimates derived here for the accretion luminosity over cosmic time we estimate the local mass density in supermassive black holes and find a good agreement with available constraints for an accretion efficiency of $\sim 10\%$. Transmission-dominated CT AGN contribute only $\sim 8\%$ to total black hole growth.

Subject headings: galaxies: active, Seyfert; X-rays: galaxies, diffuse background

1. INTRODUCTION

It is now clear that most accretion of mass onto supermassive black holes is obscured from our view (e.g., Fabian 1999; Treister et al. 2004). Observations of nearby Active Galactic Nuclei (AGN) suggested that the local ratio of obscured to unobscured sources is $\sim 4:1$ (e.g. Risaliti et al. 1999). A similarly high fraction of obscured AGN has been used to explain the spectrum and normalization of the extragalactic X-ray Background (XRB), as shown by the latest AGN population synthesis models (Treister & Urry 2005; Gilli et al. 2007). The XRB gives an integral constraint to the AGN population and its evolution; the most recent deep surveys show that $\sim 90\%$ of the observed 2–8 keV XRB radiation can be attributed to resolved AGN (Hickox & Markevitch 2006, and references therein).

The most obscured AGN known are those in which the neutral hydrogen column density (N_H) in the line of sight is higher than the inverse Thomson cross section, $N_H \simeq 1.5 \times 10^{24} \text{ cm}^{-2}$. These are the so-called Compton-thick (CT) AGN. If the obscuring column density is smaller than $\sim 10^{25} \text{ cm}^{-2}$, direct emission from the nucleus is still visible at energies greater than $\sim 10 \text{ keV}$, while the radiation at lower energies is completely ob-

scured by photoelectric absorption; in this case we have a transmission-dominated CT AGN. For sources with $N_H > 10^{25} \text{ cm}^{-2}$ the X-ray emission is significantly affected by Compton scattering at all energies, fully obscuring the direct AGN emission and leaving only the much fainter reflection component to be detected; these are reflection-dominated AGN.

Contrary to the situation for less obscured sources, not much is known about the number density of CT AGN. Thanks to the deep Chandra and XMM-Newton surveys it is now clear that the fraction of moderately obscured, Compton-thin, AGN is on average $\sim 3/4$ of all AGN, and is higher at lower luminosities (Ueda et al. 2003; Treister & Urry 2005; Barger et al. 2005) and higher redshifts (La Franca et al. 2005; Ballantyne et al. 2006; Treister & Urry 2006), but there are no comparable constraints on the number of CT AGN. About a dozen CT AGN have been identified in the local Universe (Della Ceca et al. 2008a and references therein). In fact, two of the three nearest AGN are Compton thick (NGC4945 and the Circinus Galaxy; Matt et al. 2000). Based on a sample of 49 local Seyfert 2 galaxies, Guainazzi et al. (2005) estimated that $\sim 50\%$ of all obscured AGN ($N_H > 10^{22} \text{ cm}^{-2}$) are Compton thick, and similar estimates were made by Risaliti et al. (1999) based on much smaller numbers.

However, so far there has been no systematic study of the statistical properties of CT AGN with a well-defined selection function. Hence, while it has been hypothesized that CT AGN can contribute up to $\sim 30\%$ of the XRB (Gilli et al. 2007) and represent a significant fraction of the cosmic accretion onto supermassive black holes (Marconi et al. 2004), this has not been demonstrated. Now, thanks to the wide-area surveys at high energies

¹ Institute for Astronomy, 2680 Woodlawn Drive, University of Hawaii, Honolulu, HI 96822; treister@ifa.hawaii.edu

² European Southern Observatory, Casilla 19001, Santiago 19, Chile.

³ Chandra Fellow

⁴ Department of Physics, Yale University, P.O. Box 208121, New Haven, CT 06520.

⁵ Yale Center for Astronomy and Astrophysics, P.O. Box 208121, New Haven, CT 06520.

⁶ Department of Astronomy, Yale University, PO Box 208101, New Haven, CT 06520.

performed with the INTEGRAL/IBIS (Beckmann et al. 2006; Krivonos et al. 2007) and the Swift/Burst Alert Telescope (BAT; Tueller et al. 2008), it is possible to study a well-defined sample of CT AGN in the local Universe. Furthermore, since most of the absorbed energy is re-emitted at mid-IR wavelengths, deep observations with the Spitzer observatory can be used to select CT AGN candidates at high redshift, $z \sim 2$ (Daddi et al. 2007; Fiore et al. 2008; Alexander et al. 2008), yielding an upper limit to the number density of these sources.

In this paper we constrain the number density of CT AGN in the local Universe from high-energy observations, and at high redshift using a combination of X-ray and mid-IR data. We compare the observed numbers of CT AGN with expectations from AGN population synthesis models that explain the XRB emission and we study the degeneracies affecting these models. Finally, we compute the implied density of supermassive black holes as a function of redshift, including transmission-dominated CT accretion. When required, we assume a Λ CDM cosmology with $h_0=0.7$, $\Omega_m=0.3$ and $\Omega_\Lambda=0.7$, in agreement with the most recent cosmological observations (Spergel et al. 2007).

2. THE LOCAL SAMPLE OF CT AGN

One of the best ways to find CT AGN is by observing at high energies, namely $E > 10$ keV. The hard X-ray spectrum of a CT AGN is characterized by at least three components: an absorbed power law with an upper cutoff at ~ 300 keV (e.g., Nandra & Pounds 1994), a Compton reflection hump which peaks at ~ 30 keV (Magdziarz & Zdziarski 1995) and an iron $K\alpha$ line at ~ 6.4 keV. Not all components are clearly observed in all AGN (e.g., Soldi et al. 2005; Beckmann et al. 2004), perhaps because of the low signal-to-noise of some of the observations. One clear advantage of high-energy observations is that photoelectric absorption has minimal effects, so transmission-dominated CT AGN can be easily detected. It is only when the source becomes reflection-dominated that the emission at $E > 10$ keV is affected.

Current observations at $E > 10$ keV are available only at relatively high fluxes, and hence low redshifts, $z < 0.05$. While BeppoSAX (Boella et al. 1997) was successfully used for targeted observations of known Seyfert galaxies, it is only now thanks to the International Gamma-Ray Astrophysics Laboratory (INTEGRAL; Winkler et al. 2003) and Swift (Gehrels et al. 2004) satellites that large-area surveys at these energies have been done.

Using the IBIS coded-mask telescope (Ubertini et al. 2003), INTEGRAL surveyed $\sim 80\%$ of the sky down to a flux of 5 mCrab in the 17-60 keV. The catalog of Krivonos et al. (2007) reports the properties of 130 sources detected in these all-sky observations and classified as AGN. A large number of unidentified sources remain in this catalog, 48, but only seven are found a high galactic latitude ($|b| > 5^\circ$), and thus of likely extragalactic origin. Five of the 130 AGN are CT AGN.

We carried out a very deep survey with INTEGRAL/IBIS, with a total exposure time of ~ 3 Msec, in the XMM-Large Scale Survey (XMM-LSS) region, reaching a flux limit of $\sim 3 \times 10^{-12}$ erg $\text{cm}^{-2}\text{s}^{-1}$ in the 20-40 keV band (S. Virani in prep.). A total of 15 sources, all AGN, are found in this survey, including the prototypical CT AGN, NGC 1068. We also found another CT

AGN candidate, not detected in X-rays before. However, an accurate N_H determination has not been obtained for this source yet, and hence it is not included in our sample. NGC 1068 was also included in the catalog of Krivonos et al. (2007) and hence is already in our sample.

Recently, Tueller et al. (2008) presented a catalog of 103 AGN detected in an all-sky survey with the Swift/BAT telescope. The 14 sources classified as blazars and BL Lac were excluded from our sample. 89 of the remaining AGN are at high galactic latitudes, $|b| > 15^\circ$, where only one source remains unidentified. The fraction of unidentified sources is much smaller for Swift compared to INTEGRAL because of follow-up observations with Swift's dedicated X-ray telescope. In the Tueller et al. (2008) catalog there are five AGN with estimated N_H greater than 10^{24} cm^{-2} . However, we caution that these N_H measurements were obtained by fitting a single absorbed power-law to the X-ray spectrum, while it is known that heavily absorbed AGN have more complex spectra (e.g., Vignati et al. 1999; Levenson et al. 2006).

We added to our sample the source NGC 7582, which has $N_H \sim 10^{23}$ cm^{-2} in Tueller et al. (2008) but has been shown with XMM/Newton data to have a very complex spectrum with strong evidence for mildly Compton-thick absorption, $N_H \sim 10^{24}$ cm^{-2} (Piconcelli et al. 2007). With the improved sensitivity of the Suzaku telescope (Mitsuda et al. 2007), it is possible to perform detailed X-ray spectroscopy for some of the sources detected by Swift/BAT included in the catalog of Tueller et al. (2008), revealing in some cases Compton-thick absorption. We added to our sample the source NGC 5728, which as reported by Comastri et al. (2007) from Suzaku observations is obscured by a Compton-thick gas with $N_H \simeq 2.1 \times 10^{24}$ cm^{-2} . We also added the source ESO 005-G004 which based on the Suzaku observations reported by Ueda et al. (2007) is a heavily obscured, CT AGN.

In summary, INTEGRAL and Swift found 130 and 103 AGN, respectively, in their wide area surveys; 76 sources ($\sim 58\%$) were detected by both surveys. (This fraction is not larger due to the differences in sky coverage and the non-uniform depth of the observations.) We then found 15 AGN in deep 3 Msec INTEGRAL observations, one of them the CT AGN NGC1068. INTEGRAL detected five CT AGN, while Swift found eight. However, there is incomplete overlap between the two samples and we note that the disparate energy ranges make direct comparison of fluxes difficult. The INTEGRAL-detected CT sources are: NGC4945, Circinus, Markarian 3, NGC3281 and NGC1068; the Swift/BAT CT AGN are: NGC4945, Markarian 3, NGC3281, NGC7582, NGC5728, NGC5252, NGC6240 and ESO 005-G004.

The number of CT AGN found by these surveys is surprisingly low, compared to the sample of known CT AGN in the local Universe. In a study of optically-selected Seyfert 2 galaxies with hard X-ray information, Risaliti et al. (1999) found 16 CT AGN in a total of 45 Seyfert galaxies, although four were later demonstrated to most likely not be Compton thick (NGC 1386, IC 3639, NGC 5005 and NGC 4939; Maiolino et al. 1998; Ghosh et al. 2007; Gallo et al. 2006). Of the remaining 12 CT sources, three were detected by Chandra and/or

XMM, while the rest are mostly reflection-dominated sources, too faint to be detected by either INTEGRAL or Swift even though they are nearby, moderate luminosity AGN. In fact, Awaki et al. (2008) recently confirmed the CT nature of NGC 2273, one of the sources in the Risaliti et al. (1999) sample, which is however too faint to be detected by INTEGRAL or Swift.

Recently, Della Ceca et al. (2008a) published a list of 18 CT AGN with detections at $E > 10$ keV. Of these, seven were detected by Swift and/or INTEGRAL, while the remaining 11 were studied with pointed BeppoSAX observations, and are typically fainter than the INTEGRAL/Swift detection threshold. We use all these samples, suitably amended as necessary, to place constraints on the number density of CT AGN.

An alternative way to find CT sources is by studying the water maser emission in AGN. Because large amounts of molecular gas are required to produce the maser amplification, AGN with detected water maser emission are in general heavily obscured along the line of sight. In fact, Greenhill et al. (2008) recently reported that from a sample of 42 AGN known to show water maser emission, 95% have $N_H > 10^{23}$ cm $^{-2}$ and 60% are Compton-thick. Since these AGN were not detected at high energies by either INTEGRAL or Swift we do not include them here; however, we note that water maser emission appears to be a highly efficient way to identify a large number of heavily obscured sources.

2.1. The Log N -log S Distribution

Figure 1 shows the cumulative number counts of AGN, with CT sources shown separately, as a function of hard X-ray flux. In order to avoid the necessity of specifying a standard spectrum to convert fluxes to different energy bands, we show the INTEGRAL and Swift sources separately, but note that a good agreement (within $\sim 40\%$) in the normalization between the two distributions exist if a standard band conversion is assumed. At these high fluxes the slope of the log N -log S is Euclidean, implying an uniform spatial distribution, as expected given the low redshifts of these sources. We also compare with the distribution predicted by the AGN population synthesis model with which Treister & Urry (2005) fit the XRB, and find in general good agreement in slope and normalization.

The log N -log S relations for the five CT AGN detected by INTEGRAL and the eight sources observed by Swift/BAT are also consistent with Euclidean slopes, with normalizations of 10^{-4} deg $^{-2}$ at fluxes of $\sim 5 \times 10^{-11}$ and $\sim 9 \times 10^{-11}$ erg cm $^{-2}$ s $^{-1}$ in the INTEGRAL and Swift bands, respectively. (For a power law spectrum with $\Gamma = 1.8$, for example, $F_{14-195, \text{Swift}} \sim 2.3 F_{17-60, \text{INTEGRAL}}$ for most column densities $N_H \lesssim 24$ cm $^{-2}$.) About twice as many CT AGN at low redshifts were reported in the sample of Risaliti et al. (1999). Since all these CT AGN have detections at high energies, we plot them in Fig. 1. Clearly, they fall significantly below the extrapolation of the observed log N -log S , suggesting high levels of incompleteness in the Risaliti et al. (1999) sample. This is not surprising given that these sources do not come from a flux-limited survey but from pointed observations.

A possible source of incompleteness in our sample of CT AGN comes from the difficulty in measuring

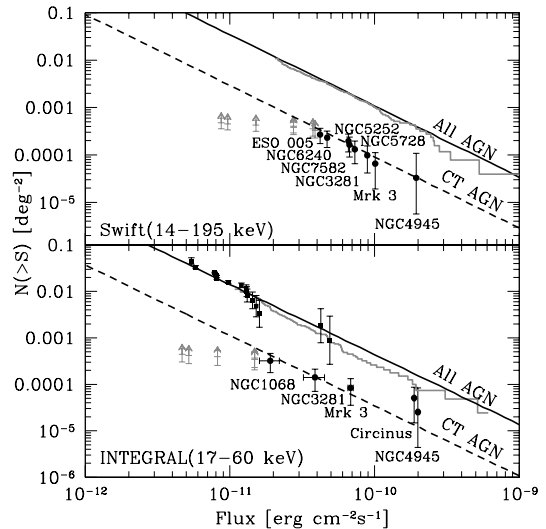


FIG. 1.— Log N -log S distribution for AGN detected at high energies. The gray line in the top panel shows the AGN in the well-defined Swift/BAT samples in the 14-195 keV band (Tueller et al. 2008), while the bottom panel shows the INTEGRAL sources (Krivonos et al. 2007) in the 17-60 keV band. Solid squares show the 15 sources detected in the deep 3 Msec INTEGRAL observations of the XMM-LSS field (S. Virani in prep.). Solid circles mark the CT AGN detected with Swift (top panel) and INTEGRAL (bottom panel). The black solid lines show the expected AGN log N -log S from the population synthesis model of Treister & Urry (2005), which at these fluxes corresponds to a Euclidean distribution. The dashed lines mark the Euclidean slope normalized to the number of Swift and INTEGRAL CT AGN. The gray lower limits show the previously-known transmission-dominated AGN with hard X-ray observations, not detected in the INTEGRAL or Swift surveys. These are lower limits since they were selected from pointed observations and are thus highly incomplete.

the amount of absorption in these sources, given that they have in general very complex X-ray spectra. As noted by Tueller et al. (2008), sources that are not well-characterized in X-rays by an absorbed power-law are good candidates to be heavily obscured AGN. In their Swift/BAT sample, a total of 46 sources with complex spectra were reported. Of those, 18 have an optical classification of Seyfert 1.5 or lower, and hence it is very unlikely that they are CT AGN. Considering the very extreme assumption that the remaining 28 sources are all CT AGN increases the normalization of the CT AGN log N -log S by only a factor of ~ 2 . This is because a large fraction of the complex-spectrum sources have fluxes fainter than that of NGC6240, one of the faintest confirmed CT AGN in the Swift sample. In any case, it is important to remark that according to a detailed study by Winter et al. (2009), while all these complex-spectrum sources are highly obscured, only half a dozen have some evidence of Compton-thick column densities. Hence, we conclude that the observed log N -log S is not affected significantly by this possible source of incompleteness.

For the transmission-dominated AGN in our sample (i.e., excluding NGC1068), we find volume densities for $L_X > 10^{42}$ erg s $^{-1}$ of $5.5^{+8.6}_{-3.1} \times 10^{-5}$ Mpc $^{-3}$; and for $L_X > 10^{43}$ erg s $^{-1}$ of $2.2^{+2.9}_{-1.1} \times 10^{-6}$ Mpc $^{-3}$. Because this is a flux-limited sample, luminosity and redshift are

strongly correlated. For example, a source with X-ray luminosity of 10^{42} , 10^{43} or 10^{44} erg s $^{-1}$ can only be detected up to $z \simeq 0.005$, 0.015 or 0.045 , respectively. Thus, the source densities inferred here are valid only up to these limiting redshifts, corresponding to distances of ~ 21 , 63 and 190 Mpc. Also, because there is a significant correlation between luminosity and fraction of obscured sources (e.g., Ueda et al. 2003; Barger et al. 2005), CT AGN are found only up to $z=0.024$ in this sample, even though unobscured sources have been found by Swift/BAT up to $z \sim 0.1$. That is, CT AGN preferentially have low luminosities, so they are found mostly at low redshift. In effect, the flux limit prevents us from detecting the many CT AGN at higher redshift. The derived volume densities for CT AGN at $z \simeq 0$ are fully consistent with the values derived by Della Ceca et al. (2008b) from three INTEGRAL sources only.

Taking into account the densities reported here, the number of CT AGN relative to the X-ray-selected AGN population is $5.3 \times 10^{-5} / 2.2 \times 10^{-4} = 24\%$ for sources in the $L_X = 10^{42-43}$ erg s $^{-1}$ range, while for sources with $L_X = 10^{43-44}$ erg s $^{-1}$ this fraction is $2.2 \times 10^{-6} / 2.9 \times 10^{-5} = 7.5\%$. This calculation uses the luminosity function of Ueda et al. (2003). However, similar numbers are obtained if the La Franca et al. (2005) luminosity function is used instead. Hence, the relative fraction of CT AGN decreases by about a factor of 3 for an order of magnitude increase in luminosity. For Compton-thin sources, according to Treister et al. (2008), the fraction of obscured sources ($N_H \geq 10^{22}$ cm $^{-2}$) decreases from 100% at $L_X = 10^{42}$ erg s $^{-1}$ to $\sim 60\%$ at $L_X = 10^{43}$ erg s $^{-1}$, implying a decrease of about a factor of 2. Therefore, the decrease in the fraction of CT AGN is comparable to the decrease in the fraction of obscured Compton-thin AGN, a reasonable agreement given the statistical errors in our sample. This is in agreement with the conclusions of Fiore et al. (2009), who found a similar decrease in CT AGN with increasing luminosity in their high-redshift IR-selected sample.

2.2. N_H Distribution

A key ingredient in our understanding of the AGN population and of the properties of the obscuring material is the distribution of line-of-sight column densities, parametrized in terms of the neutral hydrogen column density, N_H . In Fig. 2 we show the observed N_H distribution for the sources in the Swift/BAT sample of Tueller et al. (2008) obtained from very simple spectral fitting assuming an intrinsic absorbed power-law spectrum; the distribution from the AGN population synthesis models of Treister & Urry (2005), adapted to the flux limit of the Swift/BAT sample; the distribution assumed by Gilli et al. (2007); and the distribution predicted by the galaxy evolution models of Hopkins et al. (2006).

The N_H distribution observed in the Swift sample is relatively flat, before a strong decline at $N_H > 10^{24}$ cm $^{-2}$. This decline corresponds to a relatively low number of CT AGN in this sample, as mentioned before. In contrast, the N_H distribution used in the XRB population synthesis model of Treister & Urry (2005) had roughly the same number of sources with N_H in the 10^{23} - 10^{24} cm $^{-2}$ and 10^{24} - 10^{25} cm $^{-2}$ ranges, because of an incorrect assumption about the normalization of the HEAO1-A2 X-ray background. This translates into a

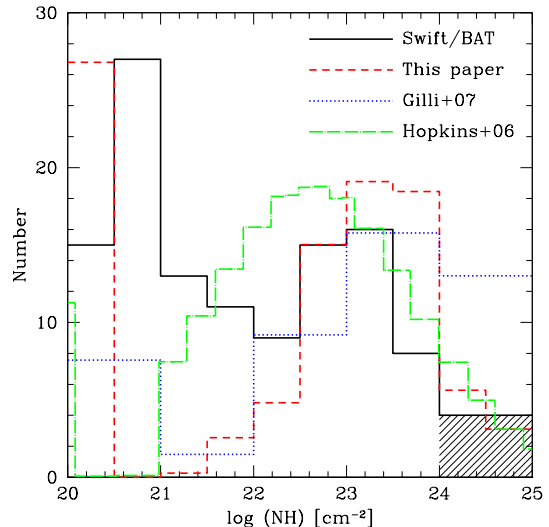


FIG. 2.— Distribution of neutral hydrogen column density (N_H) for the AGN detected in the Swift/BAT survey (*solid histogram*). The distribution is to first approximation flat, but shows a significant decrease in the number of AGN with $N_H > 10^{24}$ cm $^{-2}$. The *dotted histogram* shows the N_H distribution used in the Gilli et al. (2007) AGN population synthesis model, normalized to the number of sources in the Swift/BAT survey, while the *dot-dashed line* shows the N_H distribution predicted by the galaxy-merger models of Hopkins et al. (2006). The *dashed histogram* shows the N_H distribution assumed by the Treister & Urry (2005) model for $10^{20} < N_H < 10^{24}$ cm $^{-2}$, modified for the flux limit of the Swift/BAT survey and normalized to the same number of sources. The discrepancies at low N_H are not relevant to the present work (see §2.2 for details). For $N_H > 10^{24}$ cm $^{-2}$, the *dashed region* shows the number of CT AGN allowed by the current observations.

discrepancy of a factor of ~ 3 more CT AGN assumed by that model than is observed in the BAT sample. A similar unrealistically high number of CT AGN was assumed in the work of Gilli et al. (2007). The relationship between the number of CT AGN and the XRB is explored in detail in §3 below.

For relatively unobscured sources, $N_H < 10^{22}$ cm $^{-2}$, the Tueller et al. (2008) N_H distribution is significantly different from that observed in the deepest X-ray fields. For example, for the sources in the Chandra Deep Field North and South, Treister et al. (2004) reported a sharp peak at $N_H = 10^{20}$ cm $^{-2}$ and almost no AGN in the 10^{20} - 10^{21} cm $^{-2}$ range. The discrepancy at low values of N_H between the Swift/BAT and the deep fields samples could be due to the difficulty in measuring low N_H values at higher redshifts, as discussed by e.g., Akylas et al. (2006). The N_H distribution in the population synthesis model of Treister & Urry (2005) matches well the observed distribution in the Chandra deep fields, but has some significant differences with the distribution of Tueller et al. (2008). This discrepancy however is not relevant for our present work, which focuses on the most obscured AGN.

2.3. Comparison with Models

The N_H distribution for AGN is predicted by the galaxy evolution models of Hopkins et al. (2006). They assumed that AGN are fueled solely by mergers of gas-rich galaxies, and the N_H distribution was derived by

integrating the amount of gas along the line of sight for the simulated galaxies. The resulting distribution peaks at $N_H \sim 10^{22.5} \text{ cm}^{-2}$ and declines strongly towards higher column densities, in reasonable agreement with the number of CT sources reported here. It is interesting to note that in the Hopkins et al. model the obscuring gas is located $\sim 100\text{-}200$ pc from the nucleus. Such a large scale for the obscuration disagrees with observations of a few nearby AGN using near-IR interferometry, which show outer radii for the obscuring material of ~ 3 pc for NGC1068 (Jaffe et al. 2004) and ~ 2 pc for the Circinus galaxy (Tristram et al. 2007), for example. Similarly, the latest torus models predict small scales for the obscuring material, ≤ 10 pc (Nenkova et al. 2008b), although fitting the IR AGN spectra does not provide a very strong constraint to the torus size. Further comparisons will provide an interesting test of the Hopkins et al. model.

The fact that a relatively small number of AGN with $N_H > 10^{24} \text{ cm}^{-2}$ is observed can be used to constrain the nature of the obscuring material. This lack of CT AGN can be interpreted either in the context of a clumpy torus (e.g., Krolik & Begelman 1988; Nenkova et al. 2008a) or a smooth distribution (e.g., Pier & Krolik 1992). For example, the N_H distribution of Treister & Urry (2005), presented in Fig. 2, assumed a smooth torus with a single equatorial column density of 10^{25} cm^{-2} . To accommodate a smaller number of CT AGN while still matching the observed N_H distribution for Compton-thin sources would require a distribution of equatorial densities, in which only a small fraction of the AGN reach the CT levels for nearly-equatorial line of sights. In the case of a clumpy torus, the explanation is perhaps more natural; the small fraction of CT AGN implies that only a few sources have a large number of clouds, e.g., > 10 clouds for the models of Nenkova et al. (2008a).

3. CT AGN AND THE X-RAY BACKGROUND

3.1. Parameter Degeneracies

The spectrum of CT AGN at high energies, even for transmission-dominated sources, is often dominated by the Compton reflection component (e.g., Matt et al. 2000), which has a strong peak at $E \sim 30$ keV (Magdziarz & Zdziarski 1995). The observed spectrum of the XRB, which we now know is just the integrated emission from previously unresolved AGN, also has a peak at about the same energy (Gruber et al. 1999). Hence, it was suspected for a long time that CT AGN provide a significant contribution to the XRB emission. In fact, in the early work of Comastri et al. (1995) the contribution of CT AGN to the XRB is $\sim 20\%$, similar to the value assumed in the population synthesis models of Ueda et al. (2003), Treister & Urry (2005), and Gilli et al. (2007); Shankar et al. (2009) report a slightly higher contribution of $\sim 30\%$ at ~ 20 keV.

Because it is very hard to measure the number density of CT AGN, even locally, AGN population synthesis models have assumed it to be a fixed fraction of the obscured, Compton-thin sources, typically $\sim 0.5\text{-}1$ times as many. In Figure 3 we show the fraction of all AGN that are Compton-thick, compared to the observed fraction in the INTEGRAL and Swift samples as a function of hard X-ray flux. At fluxes of $\sim 10^{-11} \text{ erg cm}^{-2} \text{ s}^{-1}$ the fraction of CT AGN in the model of Gilli et al. (2007) is $\sim 15\%$, while the observed value is $\sim 6 \pm 5\%$ for INTEGRAL, and

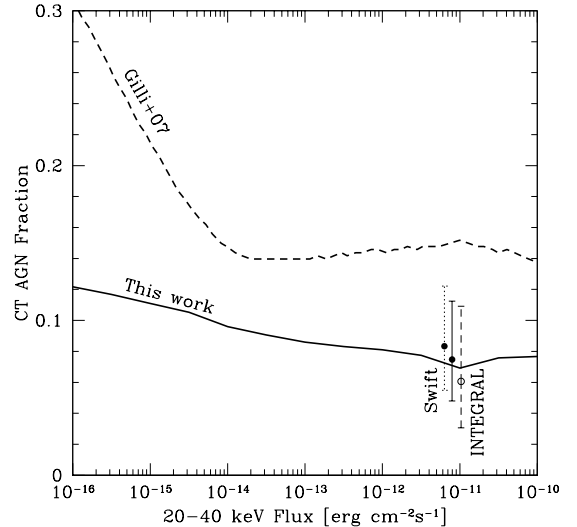


FIG. 3.— Measured fraction of AGN that are Compton-thick in the INTEGRAL (*open circles*; Krivonos et al. 2007) and Swift/BAT (*filled circles*; Tueller et al. 2008) samples. The filled circle with solid error bars shows the fraction using the identified sources only, while the circle with dotted error bars assumes that the one unidentified source is a CT AGN. The *solid line* shows the fraction of CT AGN from the modified Treister & Urry (2005) population synthesis model; the original assumption was a factor of ~ 4 too high, so was modified as described in the present text to match the Swift/BAT and INTEGRAL observations. The *dashed line* shows the fraction of CT AGN in the model of Gilli et al. (2007), which is a factor of ~ 3 higher than observations, and increases sharply at faint fluxes because of the assumed steep dependence of the fraction of obscured sources on luminosity.

$\sim 8 \pm 3\%$ for the Swift sample. For comparison, in Figure 3 (solid line) we show the predicted CT AGN fraction as a function of flux for the model of Treister & Urry (2005) with the number of CT AGN modified to match the INTEGRAL and Swift observations presented here. The Treister & Urry (2005) model assumes a nearly constant fraction of CT AGN, while the Gilli et al. (2007) model assumes a steep increase in the number of CT AGN at fluxes fainter than $\sim 10^{-14} \text{ erg cm}^{-2} \text{ s}^{-1}$. This is due to the assumed luminosity dependence of the fraction of obscured sources in the Gilli et al. (2007) model, which decreases steeply above luminosities of $\sim 10^{43} \text{ erg s}^{-1}$ and is flat at lower luminosities. While such faint fluxes are still out of reach for current hard X-ray observatories, it will be possible to test this flux regime with NuSTAR and the International X-ray Observatory (IXO). However, the luminosity dependence of the fraction of obscured AGN assumed by the model of Gilli et al. (2007) can already be ruled out, in particular at high luminosities, by observations of Compton-thin AGN at lower energies (Hasinger 2008; Treister et al. 2008).

The fact that the XRB does not constrain the number density of CT AGN can be explained by strong degeneracies in other parameters, like the assumed spread in spectral index (Gilli et al. 2007; Shankar et al. 2009), high-energy cutoff, etc. When trying to constrain the number density of CT AGN the most important parameter is the normalization of the Compton reflection component, which is directly related to the AGN luminosity at ~ 30 keV, where the CT AGN contribu-

tion is maximal. Given that even the nearest AGN have only low signal-to-noise observations at $E > 10$ keV, the normalization of the Compton reflection component is not well constrained by observations of individual sources. From a sample of 22 Seyfert galaxies, excluding CT sources, Malizia et al. (2003) concluded that both obscured and unobscured sources have similar reflection components with normalization values in the range $R \sim 0.6-1$ (in units of 2π). A similar value of $R \simeq 1$ was reported by Perola et al. (2002) based on BeppoSAX observations of a sample of 9 Seyfert 1 galaxies. Although with large scatter, normalizations for the average reflection component of 0.9 for Seyfert 1 and 1.5 for Seyfert 2 were measured from BeppoSAX observations of a sample of 36 sources (Deluit & Courvoisier 2003). Early population synthesis models for the XRB assumed values of $R=1.29$ for unobscured sources and 0.88 for obscured AGN (Comastri et al. 1995; Gilli et al. 1999). In contrast, the models of Ueda et al. (2003), Treister & Urry (2005) and Ballantyne et al. (2006) assumed a constant value of $R=1$ (equivalent to a solid angle of 2π) for both obscured and unobscured sources. Gilli et al. (2007) assumed the same normalizations as Comastri et al. (1995), $R \sim 1.3$ and 0.88; however, for high-luminosity sources, $L_X > 10^{44}$ erg s $^{-1}$, the reflection component was not included ($R=0$).

For a given number of CT AGN, the resulting intensity of the XRB at ~ 30 keV is directly linked to the assumed normalization of the reflection component. In Figure 4 we show the values of the normalization of the Compton reflection component and CT AGN number density that produce XRB intensities in the 20-40 keV region consistent with the latest observed values from INTEGRAL (Churazov et al. 2007) and Swift (Ajello et al. 2008). This is the energy range in which the contribution of CT AGN to the XRB is maximal and hence can be best constrained. For comparison, the parameters assumed by the model of Gilli et al. (2007) lie in the upper left region of Figure 4, at a density of CT AGN roughly $3\times$ higher than the observed value of $\sim 2 \times 10^{-6}$ Mpc $^{-3}$ and average Compton reflection component normalization of ~ 0.6 . (The latter is a rough estimate, since they assumed $R = 0.88$ for obscured sources at low-luminosities, and $R = 0$ at high luminosities.) The model of Treister & Urry (2005) assumed a similarly high number of CT AGN and a higher normalization of the Compton reflection component, and hence resulted in a higher intensity of the XRB, consistent with the HEAO-1 (Gruber et al. 1999) measurements increased by 40%, similar to what was assumed by Ueda et al. (2003) and Ballantyne et al. (2006) in order to match the observations of the XRB at lower energies by Chandra and XMM. Such a high value of the XRB intensity at $E \sim 10-50$ keV is now ruled out by new INTEGRAL (Churazov et al. 2007), Swift (Ajello et al. 2008) and BeppoSAX (Frontera et al. 2007) data. Given the degeneracies with other model parameters, it is unlikely that the XRB could be used to constrain the average value of R . High signal-to-noise observations of individual sources at $E > 10$ keV are required for this purpose.

3.2. A New X-ray Background Fit

Since both the number density of CT AGN and the normalization of the Compton reflection component can

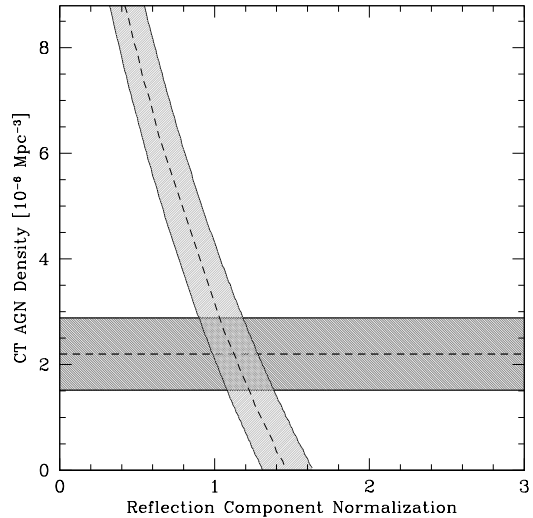


FIG. 4.— Degeneracy of the local density of CT AGN and the normalization of the Compton reflection component subject to the constraint of either the XRB intensity or the number of CT AGN in hard X-ray surveys. The *dark gray region* shows the space density obtained from the 10 CT AGN detected by Swift and INTEGRAL in complete samples at $z \sim 0$, including $1\text{-}\sigma$ statistical fluctuations. The *light gray region* shows the constraints to these parameters given by the intensity of the XRB in the 20-40 keV band, assuming a 5% uncertainty in the XRB intensity. The correct values of these parameters must be at the intersection between these two regions, namely, a normalization of the Compton reflection component of ~ 1 and a CT number density of $\sim 2 \times 10^{-6}$ Mpc $^{-3}$.

now be constrained independently, we can attempt to match the observed spectrum and intensity of the XRB. In Figure 5, we show our new fit, which matches the INTEGRAL and Swift observations at $E > 10$ keV, which are $\sim 10\%$ higher than the HEAO-1 normalization. The original fit of Treister & Urry (2005), which has a factor of ~ 4 more CT AGN, is also shown. Not surprisingly, the effects of changing the number of CT AGN are most important in the $E=10-100$ keV region.

The new XRB fit matches both the INTEGRAL and Swift/BAT observations at $E > 10$ keV and the Chandra measurements at lower energies (which are $\sim 30\%$ higher than the HEAO-1 A2 observations). Recently, a new measurement of the XRB intensity at $E=1.5-7$ keV using the Swift XRT (X-ray telescope) was presented by Moretti et al. (2009). These new data confirmed that the original HEAO-1 normalization should be increased by $\sim 30\%$ and $\sim 10\%$ at low and high energies respectively. In contrast, the AGN population synthesis model of Gilli et al. (2007) assumed the original HEAO-1 intensity at all energies, which translates into a relatively lower contribution from unobscured sources. In order to produce the necessary hard spectrum, Gilli et al. (2007) had to assume a relatively high number of obscured sources at high luminosities, i.e., an unusual, inverted dependence of the obscured fraction of AGN as a function of luminosity (Hasinger 2008; Treister et al. 2008).

Assuming a fixed value of the Compton reflection component, how much can the number of CT AGN change and still match the XRB, given the existing uncertainties in the intensity measurements? The INTEGRAL

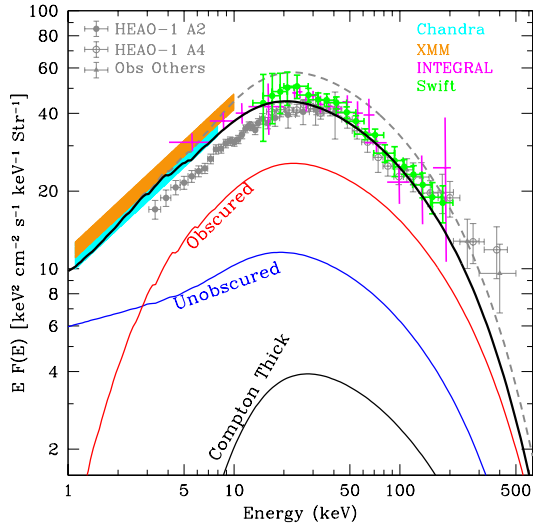


FIG. 5.— Observed spectrum of the extragalactic X-ray background from HEAO-1 (Gruber et al. 1999), Chandra (Hickox & Markevitch 2006), XMM (De Luca & Molendi 2004), INTEGRAL (Churazov et al. 2007) and Swift (Ajello et al. 2008) data. The *dashed gray line* shows the XRB spectrum from the AGN population synthesis model of Treister & Urry (2005), which assumed a 40% higher value for the HEAO-1 XRB normalization. The *thick black solid line* shows our new population synthesis model for the XRB spectrum; the only change is the number of CT AGN, which is reduced by a factor of 4 relative to the number in Treister & Urry (2005). *Red, blue* and *thin black* solid lines show the contribution to this model from unobscured, obscured Compton thin and CT AGN respectively.

measurements of the XRB, reported by Churazov et al. (2007), have uncertainties of $\sim 5\%$ including both statistical and systematic effects. Similarly, the Swift measurements have estimated errors of $\sim 3\%$ (Ajello et al. 2008). Both measurements are consistent with each other but are $\sim 10\%$ higher than the original HEAO-1 intensity. Translating this $\sim 5\%$ uncertainty into an uncertainty in the number of CT AGN, we conclude that the total number of CT AGN can be changed by a factor of 55% and still be consistent with the current measurements of the XRB. However, this calculation does not include the uncertainty in the normalization of the Compton reflection component, which is by far the dominant factor. For comparison, the statistical errors for the measurement of the ten CT AGN detected combining the Swift and INTEGRAL surveys correspond to an uncertainty of $\sim 30\%$ (Gehrels 1986), i.e., the direct detection of CT AGN is much better than the XRB for determining the number of CT AGN.

Given that the number of CT AGN in the local Universe is effectively constrained by the Swift and INTEGRAL surveys, it is now possible to estimate the total contribution of CT AGN to the XRB, as well as its redshift dependence. In order to do that, we integrate the total X-ray emission from the CT AGN in our population synthesis model and divide it by the observed XRB intensity. To facilitate the comparison with the local sources observed by Swift, and to make sure that the effects of absorption are negligible, we perform this integration over the 14-195 keV band. In Figure 6 we show

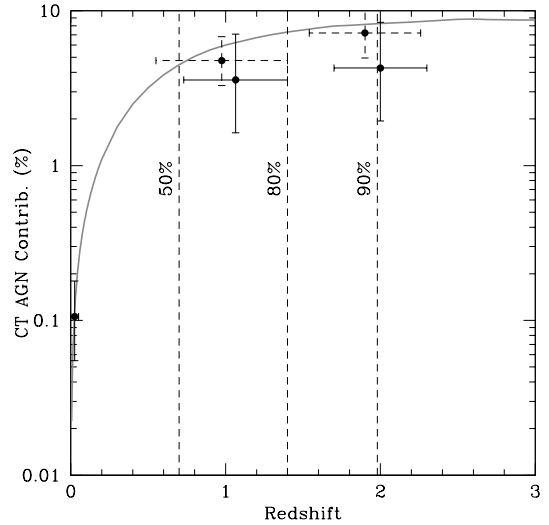


FIG. 6.— Cumulative fractional contribution of CT AGN to the XRB in the 14-195 keV Swift/BAT band as a function of redshift, from the population synthesis model presented here (*solid line*; see text for details). As shown by the vertical dashed lines, 50%, 80% and 90% of the total CT AGN contribution come from sources at $z < 0.7$, 1.4 and 2.0 respectively. Only $\sim 1\%$ of the total XRB intensity comes from CT AGN at $z > 2$. Given the current 5% uncertainties in the measurement of the XRB intensity, this means that the XRB spectrum does not constrain the number of high-redshift CT AGN at all (factor of 5 uncertainty). The data point at $z \sim 0$ corresponds to the contribution to the XRB by the CT AGN detected by Swift/BAT, while the data points at high redshift were obtained from the CT AGN in the Chandra sample of Tozzi et al. (2006). Solid error bars correspond to transmission-dominated sources only, while the data points with dashed error bars include all the sources in the sample. As expected, most of the contribution to the XRB comes from the transmission-dominated sources, which are in general brighter. Good agreement between our population synthesis model and observations of CT sources is found at all redshifts.

the resulting redshift dependence of the fractional contribution to the hard XRB radiation. As can be seen, the total contribution of CT AGN to the XRB is $\sim 9\%$, and about 50% of it comes from sources at $z < 0.7$. Similarly, we conclude that $\sim 2\%$ of the XRB is provided by CT AGN at $z > 1.4$, while CT AGN at $z > 2$ only contribute $\lesssim 1\%$ to the XRB. Conversely, the 5% uncertainty in the absolute measurement of the XRB intensity translates into an uncertainty of a factor of ~ 5 in the number of CT AGN at $z > 2$. Hence, the number of CT AGN at high redshift is largely unconstrained by the XRB.

In Figure 6 we further compare this expected redshift dependence to the integrated fluxes from individually-detected CT AGN. At $z \approx 0$ we integrate the emission from the eight sources detected by Swift/BAT. At higher redshifts we use the sample of CT AGN candidates detected in X-rays in the Chandra Deep Field South reported by Tozzi et al. (2006), which includes 14 reflection-dominated AGN and six transmission-dominated AGN with $N_H > 10^{24} \text{ cm}^{-2}$. In the same field, Georgantopoulos et al. (2007) found a total of 18 CT AGN candidates, but only eight of them with

a measured N_H greater than 10^{24} cm^{-2} ; the remaining sources were selected based on their flat X-ray spectra. All six transmission-dominated CT AGN in the sample of Tozzi et al. (2006) are included in the work of Georgantopoulos et al. (2007). However, no overlap is found between the reflection-dominated CT AGN candidates reported by Tozzi et al. (2006) and the flat-spectrum sources of Georgantopoulos et al. (2007). Hence, it is possible that either selection of heavily obscured sources is highly incomplete. In order to compare properly with the local sample, in Figure 6 we show separately the contribution from the transmission-dominated AGN and from all sources in the sample of Tozzi et al. (2006). We separated the sample at $z=1.5$, to have the same number of sources in each redshift bin. As expected, most of the contribution to the XRB comes from the transmission-dominated sources, which are in general brighter in the X-ray band. The agreement at low redshift is not surprising, since by construction our model was adjusted to match the Swift/BAT observations. However, it is very interesting that also for the high redshift sources the calculated contribution of CT AGN to the XRB agrees well with the limits from deep surveys.

4. HIGH-REDSHIFT CT AGN

As shown in the previous section, the number of CT AGN at high redshift is largely unconstrained by the XRB or by current hard X-ray surveys. Since a large fraction of the absorbed energy in heavily obscured AGN is re-emitted at mid-IR wavelengths, deep Spitzer data have been used to find CT AGN candidates at $z \geq 2$. Daddi et al. (2007) used the excess in mid-IR luminosity (compared to UV estimates of star formation rates) to find obscured AGN not individually detected in X-rays. Similarly, Fiore et al. (2008) used a combination of red optical-to-near-IR colors and high $24 \mu\text{m}$ luminosity to select CT AGN candidates at $z \sim 2$. In both cases, very high source densities have been estimated for mid-IR-selected CT AGN, e.g., Daddi et al. (2007) reported a sky density of $\sim 3,200 \text{ deg}^{-2}$, similar to that of all previously known AGN at those redshifts in the Chandra deep fields. Somewhat surprisingly, very little overlap is found between the two selection methods, implying the possible presence of interlopers. If these candidates are confirmed, a very large number of CT AGN exist at high redshift, considerably larger than the local population. This is qualitatively consistent with the evolution in obscuration detected by Treister & Urry (2006) for Compton-thin sources. Recently, Alexander et al. (2008) reported the confirmation of seven CT AGN using optical and mid-IR spectroscopy in the Chandra Deep Field North region, implying a similarly high density for CT AGN at high redshift.

In order to quantify the density of CT AGN at high redshift, and to compare with local observations and AGN luminosity functions, in Figure 7 we present the available measurements of the comoving volume density of CT AGN candidates as a function of redshift. Our measurement of the density of CT AGN at $z=0$ is $\sim 2.2 \times 10^{-6} \text{ Mpc}^{-3}$, for sources with $L_X > 10^{43} \text{ erg s}^{-1}$, as shown in §2.1. At higher redshifts and luminosities, we infer the space density from several samples. Five X-ray-selected CT AGN candidates were found

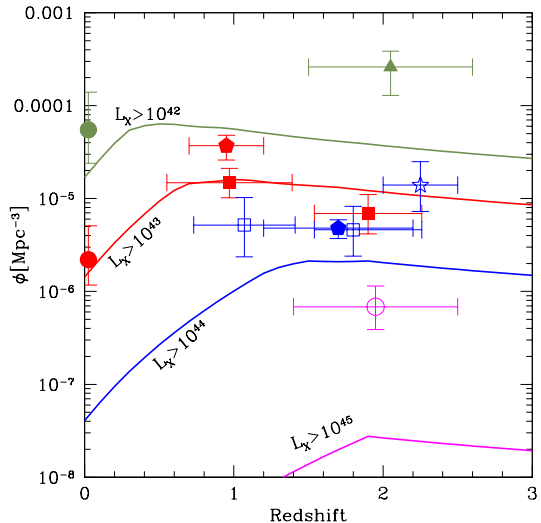


FIG. 7.— Comoving density of CT AGN as a function of redshift in several luminosity bins. Measured values (details in text) are shown by: *open circle*: Polletta et al. (2006), *squares*: Tozzi et al. (2006), *filled triangle*: Daddi et al. (2007), *pentagons*: Fiore et al. (2009), *star*: Alexander et al. (2008), *filled circle*: Swift/BAT and INTEGRAL, for luminosities limits indicated by color: *magenta*: $L_X > 10^{45} \text{ erg s}^{-1}$, *blue*: $L_X > 10^{44} \text{ erg s}^{-1}$, *red*: $L_X > 10^{43} \text{ erg s}^{-1}$ and *green*: $L_X > 10^{42} \text{ erg s}^{-1}$. *Solid lines* show the space densities at corresponding luminosities for the Treister & Urry (2005) model including the evolution of obscured AGN reported by Treister & Urry (2006), with the number of CT AGN adjusted to the observed local value (present paper). At high redshifts, a relatively large density of CT AGN is observed, compared to expectations from the evolving luminosity function. This suggests that the local sample is incomplete; or that the high-redshift infrared-selected samples include a large number of interlopers; or that CT AGN follow a different evolution than Compton-thin sources.

in the Spitzer Wide-area InfraRed Extragalactic survey (SWIRE; Polletta et al. 2006); these are transmission-dominated CT AGN and all of them have intrinsic X-ray luminosities greater than $10^{45} \text{ erg s}^{-1}$ (magenta open circle, Fig. 7). Twenty X-ray-selected CT AGN were found by Tozzi et al. (2006) in the Chandra Deep Field South; in this case, we separated the sample into two redshift bins and computed the comoving number density separately for sources with $L_X > 10^{43}$ and $L_X > 10^{44} \text{ erg s}^{-1}$ (squares, Fig. 7). Finally, we also show the comoving number density estimated from the mid-IR CT AGN candidates in the samples of Daddi et al. (2007), Fiore et al. (2009) and Alexander et al. (2008).

The expected comoving number density for CT AGN as a function of redshift was computed using the models of Treister & Urry (2005). Briefly, we used the hard (2-10 keV) X-ray luminosity function and AGN evolution of Ueda et al. (2003), with the N_H distribution and luminosity dependence of the fraction of obscured AGN of Treister & Urry (2005). In addition, we include the evolution of the relative number of obscured sources reported by Treister & Urry (2006). The normalization of the relative number of CT AGN was chosen to match the observed numbers at $z \sim 0$. This model fits the observed XRB spectral shape and normalization, as shown in Figure 5. The resulting comoving density of CT AGN as a function of redshift is shown in Figure 7 for sources with

$L_X > 10^{42}$, 10^{43} , and 10^{44} erg s $^{-1}$.

While the observed density of X-ray-selected CT AGN with $L_X > 10^{43}$ erg s $^{-1}$ is in pretty good agreement with the expectations at all redshifts, at higher luminosities the observed values are mostly higher than the expectations. In fact, the comoving density for $L_X > 10^{45}$ erg s $^{-1}$ sources from SWIRE is almost two orders of magnitude higher than the expected value. However, it is important to note that this comoving density is derived from CT AGN candidates based on the spectral properties derived from low signal-to-noise observations, and also the number of sources detected is small, so the uncertainties are large. The values for X-ray-selected CT AGN with $L_X > 10^{44}$ erg s $^{-1}$ are also higher than expectations, but in this case only by factors of ~ 2 -3. Similarly, the densities inferred from mid-IR-selected CT AGN are systematically higher than the expected values at all luminosities, typically by one order of magnitude.

This discrepancy between expectations and observations at high redshift can be interpreted in several ways. One obvious possibility is that the observations at low redshift are missing a significant number of CT AGN, which are included in the high-redshift samples. In fact, we have shown before that the high-energy surveys performed by INTEGRAL and Swift are mostly complete for transmission-dominated sources, but miss a significant fraction of the reflection-dominated AGN. While the sample of Risaliti et al. (1999) includes these sources, it is based on pointed observations and hence it is highly incomplete as well (Fig. 1). Also, it is very likely that the high-redshift IR-selected samples include both transmission and reflection-dominated sources. Another possibility is that the high-redshift samples, both X-ray- and mid-IR-selected, include a significant number of interlopers. These could be either less obscured AGN in the case of X-ray selection, or non-active galaxies undergoing significant but dusty star formation, and thus showing high mid-IR luminosities not due to AGN activity. Finally, it is possible that CT AGN follow a different evolution than Compton-thin sources. It is important to note that the $(1+z)^{0.4}$ evolution in the ratio of obscured to unobscured AGN found by Treister & Urry (2006) for Compton-thin sources is already included in the predicted volume densities. Hence, if both the low and high redshift observed samples are not systematically missing a significant number of sources, the excess of CT AGN at high redshift implies a different (stronger) evolution for these heavily obscured sources than for obscured but Compton-thin AGN.

5. THE DENSITY OF SUPERMASSIVE BLACK HOLES

Because AGN are powered by accretion of gas onto a supermassive black hole, the AGN luminosity function represents the history of cosmic accretion (Soltan 1982). Hence, the AGN bolometric luminosity can be converted into a mass accretion rate, assuming an efficiency for the conversion $\epsilon = L/\dot{m}c^2$ (typically, $\epsilon \simeq 0.1$). Then, the comoving black hole mass density can be written (following equation 17 of Yu & Tremaine 2002) as:

$$\rho(z) = \int_z^\infty \frac{dt}{dz} dz \int_{L_{min}}^{L_{max}} \frac{(1-\epsilon)BC(L_X)L_X}{\epsilon c^2} \Psi(L, z) \int_{N_{H,min}}^{N_{H,max}} f(N_H, L) dN_H \quad (1)$$

where $\Psi(L, z)$ is the evolving AGN luminosity function, $BC(L_X)$ is the bolometric correction starting from the 2-10 keV luminosity, and $f(N_H, L)$ is the “ N_H function,” or the fraction of sources at a given luminosity with a given N_H . For this calculation we used the 2-10 keV luminosity function of Ueda et al. (2003) and the N_H function with a luminosity dependence described in Section 3.2 of Treister & Urry (2005). The bolometric correction was calculated using the spectral energy distribution of a completely unobscured AGN as specified by Treister et al. (2006), as appropriate for the unified model of AGN. Additionally, we updated the spectral library with the new relation between X-ray (at 2 keV) and UV (2500Å) luminosities using the value of the slope of the power-law extrapolation reported by Steffen et al. (2006),

$$\alpha_{ox} = (-0.077 \pm 0.015) \log(L_2 \text{ keV}) + (0.492 \pm 0.387). \quad (2)$$

With these assumptions, the bolometric correction ranges from ~ 25 for $L_X = 10^{42}$ ergs s $^{-1}$ to ~ 100 for $L_X = 10^{45}$ ergs s $^{-1}$, in approximate (factor of ~ 2) agreement with the values assumed by other authors (e.g., Kuraszek et al. 2003; Marconi et al. 2004; Barger et al. 2005; Hopkins et al. 2007).

In previous works (e.g., Yu & Tremaine 2002), the AGN luminosity function was integrated from $L_{min} = 0$ to $L_{max} = \infty$, which leads to very large extrapolations in particular at the faint end. In the present case, we use the same integration limits used by Treister & Urry (2005) in their AGN population synthesis model, namely, $L_{min} = 10^{41.5}$ ergs s $^{-1}$, $L_{max} = 10^{48}$ ergs s $^{-1}$, $N_{H,min} = 10^{20}$ cm $^{-2}$ and $N_{H,max} = 10^{25}$ cm $^{-2}$. The number of CT AGN in this model is matched to the INTEGRAL and Swift results, as reported above. With these assumptions, and using the typical value of $\epsilon = 0.1$, we obtain a value for the local black hole mass density of $\rho(z=0) = 4.5 \times 10^5 M_\odot \text{ Mpc}^{-3}$. This calculation agrees well with the values estimated from observations: $\rho = 4.6_{-1.4}^{+1.9} \times 10^5 M_\odot \text{ Mpc}^{-3}$ (Marconi et al. 2004) and $\rho = (3.2-5.4) \times 10^5 M_\odot \text{ Mpc}^{-3}$ (Shankar et al. 2009).

In Figure 8 we present the black hole mass density as a function of redshift estimated from our calculation, together with the curves presented by Marconi et al. (2004) and Yu & Tremaine (2002). The main differences with the work of Marconi et al. (2004) are in the number of CT AGN (they assumed 4 times more), the assumed bolometric correction (our is ~ 3 times higher at low luminosities) and the redshift limit of the integration. Of these, the bolometric correction dominates, such that our derived local black holes mass density is slightly larger, even with the reduced number of CT AGN. Note that the bolometric correction of Marconi et al. (2004) was obtained from observations of high-luminosity sources only, while our bolometric correction was tested by observations of fainter sources as well (Treister et al. 2006). A remarkably good agreement is found between our results and the recent work of Shankar et al. (2009). Compared to Yu & Tremaine (2002), we find twice the local integrated black hole mass density, because they used an optical quasar luminosity function and evolution, which peaks at a higher redshift, $z \sim 2$, and evolves strongly. In contrast, the Ueda et al. (2003) luminosity function,

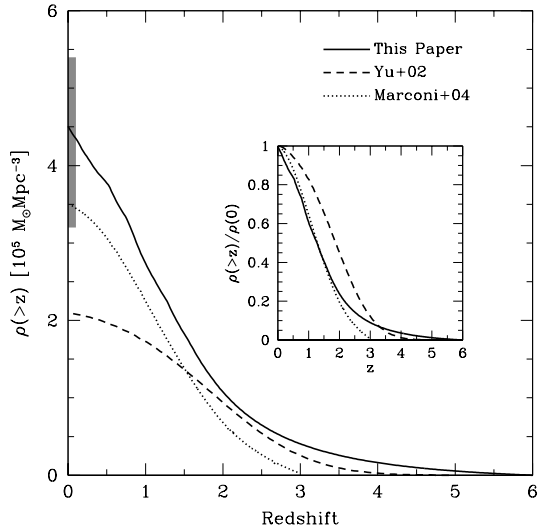


FIG. 8.— Black hole mass density as a function of redshift (inset shows the same curves normalized to their values at $z=0$), assuming an efficiency $\epsilon \equiv L/\dot{m}c^2 = 0.1$. The *solid lines* show the evolution for the population synthesis model described in this paper, while the *dotted lines* show a similar calculation presented by Marconi et al. (2004). In both cases the AGN luminosity function of Ueda et al. (2003) was used, and the only differences are the number of CT AGN (4 times more in the model of Marconi et al. 2004) and the assumed bolometric correction (~ 3 times higher for our calculation). The *gray rectangle* at $z=0$ shows the range of values consistent with observations, as reported by Shankar et al. (2009). For comparison, the *dashed lines* show the black hole mass density estimated by Yu & Tremaine (2002) which considered only high-luminosity unobscured sources.

which includes lower luminosity and obscured sources, peaks at $z \simeq 1.1$. In our calculation, the vast majority of the black hole growth occurs at low redshift ($\sim 50\%$ from $z = 1.3$ to 0), which matches observations of AGN detected in X-rays (e.g, Barger et al. 2001).

The space density of CT AGN is consistent with, but cannot be constrained by, the observed local black hole mass density. In addition, analogous to the weakness of the XRB integral constraint on the number of CT AGN, numerous degeneracies with other parameters, like the assumed bolometric correction and efficiency, are important. Even taking into account only the uncertainties in the local black hole mass density, we could still increase the number of CT AGN in the local Universe by factors of ~ 3 . Hence, we can conclude that direct observations of CT AGN at high energies, like the INTEGRAL and Swift observations discussed here, are currently the only way to constrain the population of heavily obscured supermassive black holes.

6. CONCLUSIONS

In this paper we constrain the space density of CT AGN in the local Universe using the recently-available wide-area surveys at high energies performed by INTEGRAL/IBIS and Swift/BAT. A total of ten CT AGN at $z < 0.03$ were found by either INTEGRAL and/or Swift. These observations are complete for transmission-dominated CT AGN, but are probably still missing heavily obscured sources with $N_H > 10^{25} \text{ cm}^{-2}$. We find that the space density of local CT AGN follow a Euclidean

distribution with a normalization of $\sim 10^{-4} \text{ deg}^{-2}$ at fluxes of $\sim 5 \times 10^{-11}$ and $\sim 9 \times 10^{-11} \text{ erg cm}^{-2} \text{ s}^{-1}$ in the 17-60 keV and 14-195 keV bands, respectively. This is about 3-4 times smaller than the values expected from recent AGN population synthesis models that fit the extragalactic XRB (Treister & Urry 2005; Gilli et al. 2007), and thus modifications to those models is required.

We present here a new population synthesis model for the XRB, with the number of CT AGN constrained by the INTEGRAL and Swift number counts. We find that the fraction of AGN that are Compton thick at $F_{20-100 \text{ keV}} \sim 10^{-11} \text{ erg cm}^{-2} \text{ s}^{-1}$ is $\sim 5\%$. We show that the XRB by itself cannot be used to constrain the number of CT AGN, mainly due to degeneracies with other parameters, the most important of which is the normalization of the Compton reflection component. We find that the total contribution of CT AGN to the XRB is $\sim 9\%$, with only $\lesssim 1\%$ from CT AGN at $z > 2$. Hence, taking into account the 5% uncertainty in the XRB intensity measurements, the number of CT AGN at high redshift is essentially unconstrained by the XRB, even if all the other parameters could be fixed.

We calculate the local black hole mass density inferred from AGN activity using Soltan's argument (Soltan 1982), taking into account the contribution from CT AGN estimated in this work. For an accretion efficiency $\epsilon \equiv L/\dot{m}c^2 = 0.1$, we find an integrated local black hole mass density of $4.5 \times 10^5 M_\odot \text{ Mpc}^{-3}$, in excellent agreement with recent estimates based on measured masses of local dormant black holes. Considering the current uncertainties in these estimates, we conclude that only the direct observations of CT AGN such as those discussed in this paper can effectively constrain the number of heavily obscured AGN. Based on the number density of CT AGN presented here, our best estimate of the fractional contribution of CT AGN to the total accreted black hole mass is $< 10\%$.

Using a combination of X-ray and mid-IR selection, the space density of CT AGN at high redshift is starting to be constrained. We find that observed densities are systematically higher than expected from the evolving AGN luminosity function measured from less obscured sources, assuming N_H -independent evolution of the local CT AGN population. This can be explained in three ways, any or all of which could be the case. First, the local sample might be incomplete, particularly because even hard X-ray selection is biased against reflection-dominated CT AGN. Second, the high-redshift samples may be contaminated by strongly star-forming galaxies or other interlopers. Third, CT AGN may evolve more strongly than less-absorbed sources, implying a relatively larger number of CT AGN in the early Universe. To decide this question requires the help of observations with the new generation space-based hard X-ray observatories. While mid-IR selection of heavily obscured AGN is very promising, these samples are inevitably affected by the presence of interlopers, in particular from star-forming galaxies, and by the lack of accurate measurements of the amount of obscuration.

Hard X-ray selection provides a cleaner sample of CT AGN, since N_H values can be measured directly and there is almost no contamination from star-forming galaxies at these energies. Several different approaches are currently being planned for the next generation of

high-energy ($E > 10$ keV) missions, to provide a large and complete sample of CT AGN up to $z \sim 3$. The Energetic X-ray Imaging Survey Telescope⁷ (EXIST; Grindlay 2005) will perform an all-sky survey in the 20-80 keV energy band to flux limits of $\sim 6 \times 10^{-13}$ erg cm⁻²s⁻¹, finding thousands of heavily obscured AGN up to $z \sim 1$ and high-luminosity CT quasars at all redshifts. With a complementary approach, the Nuclear Spectroscopic Telescope Array⁸ (NuSTAR; Harrison 2008), with a scheduled launch date of August 2011, will perform targeted observations of fields of ~ 1 deg² to flux limits of $\sim 2 \times 10^{-14}$ erg cm⁻²s⁻¹, hence ~ 20 times deeper than EXIST, in the 6-79 keV band, for exposure times of ~ 1 Msec; these observations will be able to find low-luminosity CT AGN up to $z \sim 2-3$. Similarly, the planned New X-ray Telescope⁹ (NeXT; Takahashi et al. 2008), scheduled for launch in 2013 will provide imaging and spectroscopy in the 5-80 keV energy band with an angular resolution $< 1.7'$ and a spectral resolution of ~ 1.5 keV. Another focusing hard X-ray observatory, Simbol-X¹⁰, is targeted for launch in 2014 (Ferrando et al. 2004). Simbol-X will perform pointed observations with a field of view of $\sim 12'$ and an angular resolution of $\sim 30''$.

Finally, it is important to note that for $z \sim 2$ the Chandra and XMM observed energy band of 2-10 keV corresponds to a rest-frame energy of $\sim 6-30$ keV, so the effects of obscuration are less important. Unfortunately even the deepest Chandra data available now only detect a few photons for the CT AGN candidates at $z \sim 2$ (e.g., Tozzi et al. 2006), thus preventing detailed spec-

tral fitting that could provide a deeper physical understanding of the nature of these sources. The proposed International X-ray Observatory¹¹ (IXO) will provide an outstanding opportunity to study these highly-obscured high-redshift sources. As reported by Alexander et al. (2008), the IXO will be able to detect thousands of photons for the CT AGN detected in the Chandra Deep Fields observations for similar, ~ 1 Msec, exposure times, yielding high signal-to-noise spectra for these sources. Deep observations at high energies with NuSTAR, EXIST and Simbol-X will provide large samples of heavily obscured AGN at $z \sim 1-3$, while the improved sensitivity and spectral resolution of the IXO will allow us to study in detail the spectra of CT AGN at $z \sim 2-3$.

We thank the anonymous referee for very useful comments. We acknowledge support from NASA/INTEGRAL grants NNG05GM79G and NNX08AE15G. Support for the work of ET was provided by the National Aeronautics and Space Administration through Chandra Postdoctoral Fellowship Award Number PF8-90055 issued by the Chandra X-ray Observatory Center, which is operated by the Smithsonian Astrophysical Observatory for and on behalf of the National Aeronautics Space Administration under contract NAS8-03060. SV acknowledges support from a graduate research scholarship awarded by the Natural Science and Engineering Research Council of Canada (NSERC).

⁷ More information about EXIST can be found at <http://exist.gsfc.nasa.gov/>

⁸ The NuSTAR website URL is <http://www.nustar.caltech.edu/>

⁹ <http://www.astro.isas.ac.jp/future/NeXT/>

¹⁰ More details can be found at <http://smc.cnes.fr/SIMBOLX/>

¹¹ <http://ixo.gsfc.nasa.gov/>

REFERENCES

- Ajello, M., et al. 2008, *ApJ*, 689, 666
 Akylas, A., Georgantopoulos, I., Georgakakis, A., Kitsionas, S., & Hatziminaoglou, E. 2006, *A&A*, 459, 693
 Alexander, D. M., et al. 2008, *ApJ*, 687, 835
 Awaki, H., Terashima, Y., Higaki, Y., & Fukazawa, Y. 2008, *PASJ* in press, arXiv:0810.4570
 Ballantyne, D. R., Everett, J. E., & Murray, N. 2006, *ApJ*, 639, 740
 Barger, A. J., Cowie, L. L., Bautz, M. W., Brandt, W. N., Garmire, G. P., Hornschemeier, A. E., Ivison, R. J., & Owen, F. N. 2001, *AJ*, 122, 2177
 Barger, A. J., Cowie, L. L., Mushotzky, R. F., Yang, Y., Wang, W.-H., Steffen, A. T., & Capak, P. 2005, *AJ*, 129, 578
 Beckmann, V., Gehrels, N., Favre, P., Walter, R., Courvoisier, T. J.-L., Petrucci, P.-O., & Malzac, J. 2004, *ApJ*, 614, 641
 Beckmann, V., Gehrels, N., Shrader, C. R., & Soldi, S. 2006, *ApJ*, 638, 642
 Boella, G., Butler, R. C., Perola, G. C., Piro, L., Scarsi, L., & Bleeker, J. A. M. 1997, *A&AS*, 122, 299
 Churazov, E. et al. 2007, *A&A*, 467, 529
 Comastri, A., Gilli, R., Vignali, C., Matt, G., Fiore, F., & Iwasawa, K. 2007, *Progress of Theoretical Physics Supplement*, 169, 274
 Comastri, A., Setti, G., Zamorani, G., & Hasinger, G. 1995, *A&A*, 296, 1
 Daddi, E., Alexander, D. M., Dickinson, M., Gilli, R., Renzini, A., Elbaz, D., Cimatti, A., Chary, R., Frayer, D., Bauer, F. E., Brandt, W. N., Giavalisco, M., Grogin, N. A., Huynh, M., Kurk, J., Mignoli, M., Morrison, G., Pope, A., & Ravindranath, S. 2007, *ApJ*, 670, 173
 De Luca, A. & Molendi, S. 2004, *A&A*, 419, 837
 Della Ceca, R., Severgnini, P., Caccianiga, A., Comastri, A., Gilli, R., Fiore, F., Piconcelli, E., Malaguti, P., & Vignali, C. 2008, *Memorie della Societa Astronomica Italiana*, 79, 65
 Della Ceca, R., et al. 2008, *A&A*, 487, 119
 Deluit, S. & Courvoisier, T. J.-L. 2003, *A&A*, 399, 77
 Fabian, A. C. 1999, *MNRAS*, 308, L39
 Ferrando, P., et al. 2004, *Proc. SPIE*, 5168, 65
 Fiore, F. et al. 2008, *ApJ*, 672, 94
 Fiore, F., et al. 2009, *ApJ*, submitted, arXiv:0810.0720
 Frontera, F., Orlandini, M., Landi, R., Comastri, A., Fiore, F., Setti, G., Amati, L., Costa, E., Masetti, N., & Palazzi, E. 2007, *ApJ*, 666, 86
 Gallo, L. C., Lehmann, I., Pietsch, W., Boller, T., Brinkmann, W., Friedrich, P., & Grupe, D. 2006, *MNRAS*, 365, 688
 Gehrels, N. 1986, *ApJ*, 303, 336
 Gehrels, N. et al. 2004, *ApJ*, 611, 1005
 Georgantopoulos, I., Georgakakis, A., & Akylas, A. 2007, *A&A*, 466, 823
 Ghosh, H., Pogge, R. W., Mathur, S., Martini, P., & Shields, J. C. 2007, *ApJ*, 656, 105
 Gilli, R., Comastri, A., & Hasinger, G. 2007, *A&A*, 463, 79
 Gilli, R., Risaliti, G., & Salvati, M. 1999, *A&A*, 347, 424
 Greenhill, L. J., Tilak, A., & Madejski, G. 2008, *ApJ*, 686, L13
 Grindlay, J. E. 2005, *New Astronomy Review*, 49, 436
 Gruber, D. E., Matteson, J. L., Peterson, L. E., & Jung, G. V. 1999, *ApJ*, 520, 124
 Guainazzi, M., Matt, G., & Perola, G. C. 2005, *A&A*, 444, 119
 Harrison, F. 2008, in *AAS/High Energy Astrophysics Division*, Vol. 10, AAS/High Energy Astrophysics Division, 40.01–+
 Hasinger, G. 2008, *A&A*, 490, 905
 Hickox, R. C. & Markevitch, M. 2006, *ApJ*, 645, 95

- Hopkins, P. F., Hernquist, L., Cox, T. J., Di Matteo, T., Robertson, B., & Springel, V. 2006, *ApJS*, 163, 1
- Hopkins, P. F., Richards, G. T., & Hernquist, L. 2007, *ApJ*, 654, 731
- Jaffe, W. et al. 2004, *Nature*, 429, 47
- Krivonos, R., Revnivtsev, M., Lutovinov, A., Sazonov, S., Churazov, E., & Sunyaev, R. 2007, *A&A*, 475, 775
- Krolik, J. H. & Begelman, M. C. 1988, *ApJ*, 329, 702
- Kuraszkiewicz, J. K. et al. 2003, *ApJ*, 590, 128
- La Franca, F. et al. 2005, *ApJ*, 635, 864
- Levenson, N. A., Heckman, T. M., Krolik, J. H., Weaver, K. A., & Życki, P. T. 2006, *ApJ*, 648, 111
- Magdziarz, P. & Zdziarski, A. A. 1995, *MNRAS*, 273, 837
- Maiolino, R., Salvati, M., Bassani, L., Dadina, M., della Ceca, R., Matt, G., Risaliti, G., & Zamorani, G. 1998, *A&A*, 338, 781
- Malizia, A., Bassani, L., Stephen, J. B., Di Cocco, G., Fiore, F., & Dean, A. J. 2003, *ApJ*, 589, L17
- Marconi, A., Risaliti, G., Gilli, R., Hunt, L. K., Maiolino, R., & Salvati, M. 2004, *MNRAS*, 351, 169
- Matt, G., Fabian, A. C., Guainazzi, M., Iwasawa, K., Bassani, L., & Malaguti, G. 2000, *MNRAS*, 318, 173
- Mitsuda, K. et al. 2007, *PASJ*, 59, 1
- Moretti, A., et al. 2009, *A&A*, 493, 501
- Nandra, K. & Pounds, K. A. 1994, *MNRAS*, 268, 405
- Nenkova, M., Sirocky, M. M., Ivezić, Ž., & Elitzur, M. 2008a, *ApJ*, 685, 147
- Nenkova, M., Sirocky, M. M., Nikutta, R., Ivezić, Ž., & Elitzur, M. 2008b, *ApJ*, 685, 160
- Perola, G. C., Matt, G., Cappi, M., Fiore, F., Guainazzi, M., Maraschi, L., Petrucci, P. O., & Piro, L. 2002, *A&A*, 389, 802
- Piconcelli, E., Bianchi, S., Guainazzi, M., Fiore, F., & Chiaberge, M. 2007, *A&A*, 466, 855
- Pier, E. A. & Krolik, J. H. 1992, *ApJ*, 401, 99
- Polletta, M. d. C. et al. 2006, *ApJ*, 642, 673
- Risaliti, G., Maiolino, R., & Salvati, M. 1999, *ApJ*, 522, 157
- Shankar, F., Weinberg, D. H., & Miralda-Escudé, J. 2009, *ApJ*, 690, 20
- Soldi, S., Beckmann, V., Bassani, L., Courvoisier, T. J.-L., Landi, R., Malizia, A., Dean, A. J., de Rosa, A., Fabian, A. C., & Walter, R. 2005, *A&A*, 444, 431
- Soltan, A. 1982, *MNRAS*, 200, 115
- Spiegel, D. N. et al. 2007, *ApJS*, 170, 377
- Steffen, A. T., Strateva, I., Brandt, W. N., Alexander, D. M., Koekemoer, A. M., Lehmer, B. D., Schneider, D. P., & Vignali, C. 2006, *AJ*, 131, 2826
- Takahashi, T., et al. 2008, *Proc. SPIE*, 7011, 18
- Tozzi, P. et al. 2006, *A&A*, 451, 457
- Treister, E. & Urry, C. M. 2005, *ApJ*, 630, 115
- . 2006, *ApJ*, 652, L79
- Treister, E., Urry, C. M., Van Dуйne, J., Dickinson, M., Chary, R.-R., Alexander, D. M., Bauer, F., Natarajan, P., Lira, P., & Grogin, N. A. 2006, *ApJ*, 640, 603
- Treister, E., et al. 2009, *ApJ* in press, arXiv:0810.3917
- Treister, E. et al. 2004, *ApJ*, 616, 123
- Tristram, K. R. W. et al. 2007, *A&A*, 474, 837
- Tueller, J., Mushotzky, R. F., Barthelmy, S., Cannizzo, J. K., Gehrels, N., Markwardt, C. B., Skinner, G. K., & Winter, L. M. 2008, *ApJ*, 681, 113
- Ubertini, P. et al. 2003, *A&A*, 411, L131
- Ueda, Y., Akiyama, M., Ohta, K., & Miyaji, T. 2003, *ApJ*, 598, 886
- Ueda, Y., Eguchi, S., Terashima, Y., Mushotzky, R., Tueller, J., Markwardt, C., Gehrels, N., Hashimoto, Y., & Potter, S. 2007, *ApJ*, 664, L79
- Vignati, P., Molendi, S., Matt, G., Guainazzi, M., Antonelli, L. A., Bassani, L., Brandt, W. N., Fabian, A. C., Iwasawa, K., Maiolino, R., Malaguti, G., Marconi, A., & Perola, G. C. 1999, *A&A*, 349, L57
- Winkler, C. et al. 2003, *A&A*, 411, L1
- Winter, L. M., Mushotzky, R. F., Reynolds, C. S., & Tueller, J. 2009, *ApJ*, 690, 1322
- Yu, Q. & Tremaine, S. 2002, *MNRAS*, 335, 965